Biointerface Research in Applied Chemistry
Open-Access Journal (ISSN: 2069-5837)

Article
Volume 13, Issue 5, 2023, 415
https://doi.org/10.33263/BRIAC135.415

Flow Transport Phenomena of a Hybrid Nanofluid Suspended by Magnetic Iron Oxide and Molybdenum Disulfide Nanoparticles in Blood Plasma

Gopi Vinayagam [1], Vijaya Kumar Avula Golla [1,*]

[1] Department of Mathematics, SAS, Vellore Institute of Technology, Vellore-632014, India; gopi.v2018@vitstudent.ac.in (G.V); vijayakumarag@vit.ac.in (V.K.A.G);
* Correspondence: vijayakumarag@vit.ac.in (V.K.A.G.);

Scopus Author ID8227441000

Received: 30.07.2022; Accepted: 3.10.2022; Published: 22.11.2022

Abstract: This present work reveals the numerical solution of two-dimensional MoS_2-Fe_3O_4/blood-based hybrid nanofluid flow over a stretching surface with affecting thermal radiation. Iron oxide (Fe_3O_4) and Molybdenum Disulfide (MoS_2) are hybrid nanoparticles that are suspended in blood plasma. This investigation provides information on the effectiveness of distinct physical quantities such as thermal radiation, dissipative viscosity, heat absorbtion, and convective heat transfer. Various parameters and their effects on temperature and velocity are examined in this explanatory paper. The explanations using graphs and numerical tables aid in understanding and strengthen interpretations of the study's findings. A flow transport model constructs coupled partial differential equations, which may be transformed into ordinary differential equations by appropriate similarity transformations. The R-K-Felhberg-integration through shooting technique is then used to elucidate the resulting equations numerically. Based on these findings, the heat transmission rate of MoS_2-Fe_3O_4/Blood is superior to that of Fe_3O_4/blood subject to thermal radiation.

Keywords: MoS_2 -Fe_3O_4/blood; magnetic field; hybrid nanofluid; heat source absorption; thermal radiation; porous medium.

Nomenclature:

B_i	Biot Number	R	Radiation Parameter
B_0	Strength of magnetic field (T)	T	Temperature of the fluid
C_{f_x}	Skin friction coefficient	T_w	Temperature of the surface (K)
C_p	Specific heat $\left(Jkg^{-1}K^{-1}\right)$	T_∞	Ambient temperature (K)
ρC_p	Heat capacity	u_w	Stretching surface velocity $\left(ms^{-1}\right)$
E_c	Eckert Number	u_∞	Mainstream velocity
$f(\eta)$	Dimensionless velocity function	α	Thermal diffusivity
k	Thermal conductivity $\left(Wm^{-1}K^{-1}\right)$	ϕ	Volume fraction
k^*	Rosseland mean absorption coefficient $\left(m^{-1}\right)$	μ	Dynamic viscosity $\left(kgm^{-1}s^{-1}\right)$
M	Magnetic field	f	Base fluid
P_r	Prandtl number	ρ	Density
Q_0	Heat source/Sink coefficient	hnf	Hybrid Nanofluid

1. Introduction

Blood is the fluid that transports oxygen, nutrients, and other metabolic wastes throughout the body to preserve cell-level metabolism, regulate the human body's pH, osmotic pressure, and temperature, and protect it from microbial and mechanical harm. Human blood, which comprises erythrocytes, leukocytes, and platelets suspended in plasma, is a Newtonian fluid that is heterogeneous and polyphasic. However, due to the suspension, the entire blood has non-Newtonian fluid characteristics, which substantially alters natural philosophy aspects. The flow of the blood traveling through massive blood vessels Newtonian behavior may be presumed. On the other hand, blood has a non-Newtonian nature in narrow arteries or capillaries. Blood is employed as a testing medium since the medications are made in the form of a hybrid nanofluid. In addition, hybrid nanofluid is improving the thermal efficiency of the base fluid. Normal viscosity and temperature are required for superior blood circulation to promote consistency in blood transmission. The nanoparticles are widely employed in food products, medical science, nuclear furnace, farming, and other fields. The primary convectional fluids, like air, oils, H_2O, $C_2H_6O_2$, etc., have the lowest thermal conductivity. Therefore nanofluids are discovered for better thermal conductivity.

The name nanofluid was early proposed by Choi [1, 2] and is explained as the fluids between 1-100 nm in size disseminated in the base fluid. From the early 1990s onwards, numerous nanofluid research papers have been published. Eshetu Heile *et al*. [3] studied two types of nanofluids Cu/water and Al_2O_3 /water by means of portable permeable surface and described Blasius and Sakiadis velocity profiles for both Cu and Al_2O_3. The influence of radiation on Copper (Cu)-water and Silver (Ag)-water nanofluids on a stretching surface a constant for stable magnetohydrodynamics investigation was conducted numerically by Elazem *et al*. [4] and discovered that Silver (Ag)-water nano liquid has greater thermal conductivity and temperature than Copper (Cu)-water nano liquid. Gaikwad *et al*. [5] investigated two different types of nano liquids, Cu-water and CuO-water, over the vertical permeable stretched flat plate with a heat source and noticed that the Copper-water nanofluid is effectively embellishing heat transfer with Copper oxide-water nanofluid. The numerical investigation of three different nanofluids, Aluminium oxide/water, Copper oxide/water, and Copper/water flow through a square cross-cut pipe, was deliberated by Heris *et al*. [6] and observed that Copper-water has higher energy transfer characteristics. In contrast, Copper Oxide-water has a moderate energy transfer rate, and Aluminium Oxide-water has the lowest energy transfer rate. Further, numerical analysis of the free convective transmission of heat characteristics of Ag-water nano liquid in a cage with the center heater at both horizontal and vertical positions has been explored by Nithyadevi *et al*. [7].

However, the researcher is searching for an advanced type of nanofluid, such as a hybrid nanofluid. A Hybrid nanofluid is a mixture of two or more different particles of nanometre size with base fluids and has better thermal conductivity enhanced heat transfer than nanofluids. Recently Indumathi *et al*. [8] investigated three different types of hybrid nanofluids, Al_2O_3-TiO_2/H_2O, Al_2O_3-SiO_2/H_2O, and TiO_2-SiO_2/H_2O with Marangoni boundary constraints and observed that Al_2O_3-TiO_2/H_2O has higher temperature rate than Al_2O_3-SiO_2/H_2O and TiO_2-SiO_2/H_2O. Anjali Devi *et al*. [9] investigated hydromagnetic hybrid nano liquid Cu-Al_2O_3/water through an absorbing stretching surface under the nose of a magnetic field numerically and discovered that the thermal energy rate of Copper-Aluminium Oxide /water is greater than that of Copper/water in magnetic flux. Rajesh *et al*. [10] deliberated the unstable

free convection boundary layer stream of Copper-Aluminium Oxide/water caused due to stretching surface under the influence of magnetohydrodynamic effects. Rusya Iryanti Yahaya *et al*. [11] investigated the stream and energy dissipation of a hybrid nanofluid Copper-Aluminium Oxide/water through an absorbing stretching or shrinking surface. W.Alghamdi *et al*. [12] investigated the flow of Copper-Copper Oxide/Blood hybrid nano liquid with coupling stress over a permeable path through a rectangular field and discovered the pressure dispersion while the drug consignment maintained the vessel's blood flow stability. The stability and numerical solutions of 3D rotating hybrid nanofluid (Cu-Al_2O_3/Water) flow have been studied by Nursya Zana Anuar *et al*. [13]. And produced a non-unique solution when $\lambda \le -1$, the distinct solution has been observed when $\lambda > -1$ and no solutions exist otherwise. Iskandar Waini *et al*. [14] looked into a hybrid nanofluid (Cu-Al_2O_3/H_2O) over a permeable, non-uniformly stretching and shrinking surface with consequences of thermal radiation. Nursyahirah Wahid *et al*. [15] have recently scrutinized a hybrid nanofluid (Alumina-copper/water) slipstream caused by a stretching and shrinking surface that can generate heat exponentially. Afterward, Muhammad Ijaz Khan *et al*. [16] examined entropy optimization in magnetohydrodynamic hybrid nanofluid (SiO_2-MoS_2/$C_3H_8O_2$) flow towards a stretchable surface. Investigation of Marangoni hybrid nanofluid (Cu-Al_2O_3/Water) protective layer flow over a bibulous infinite disc plunged in a porous medium was studied by Nursyahirah Wahid *et al*. [17]. Nurul Amira Zainal *et al*. [18] have recently studied an unsteady hybrid nano liquid (Alumina–copper/water) at the point of stagnation with the inclusion of electro magneto hydrodynamic over a stretching/shrinking sheet. The consequential effects of absorption and magnetic field through a moving plate of a hybrid nano liquid Cu-Al_2O_3/water were examined numerically by NuradilahLiyana Aladdin *et al*. [19]. Aly and Pop [20] investigated magnetohydrodynamics, thermal radiation, and mixed convection of the wall jet flow for a hybrid nanofluid Cu-Al_2O_3/water over a vertical plate. The heat transfer and rheological properties of (Ag-CuO/water) through a moving oscillating cylinder were explored numerically by Rajesh *et al*. [21], who noticed that Ag-CuO/water achieves superior temperatures but lower velocities than CuO/water.

Hamza Babar *et al*. [22] discussed the Preparation, Thermophysical properties, diligence, and contradictions of hybrid nanofluid. Suresh *et al*. [23, 24] empirically scrutinized the Al_2O_3-Cu nanocomposite powder developed by thermochemical process and Al_2O_3-Cu/water proposed by scattering the enzymatic nanocomposite powder in purified H_2O. Theoretical and software development results in a problem-solving environment that allow them to solve boundary value problems faster has been explained by Jacek and Shampine [25]. Hayat *et al*. [26] explored3-D the magnetohydrodynamic flow of circulatory hybrid nanofluid Ag-CuO/water over a stretching field with heat propagation or suction effects. Afterward, Nadeem *et al*. [27] studied the heat transmission of a hybrid nanofluid within the sight of nanoparticles of SWCNT-MWCNT over a 3-D convectively heated stretching environment. The MHD flow and heat transmission of hybrid nano liquid Cu-Al2O3/water suspended in the micropolar grubby fluid under the nose of shapes nanoparticles analysis has been made by Hosseinzadeh *et al*. [28]. Afridi *et al*. [29] have scrutinized the Blasius (infinite static plate) and Sakiadis (moving flat plate) flows of hybrid nanofluids Cu-Al_2O_3/H_2O and Cu-Al2O3/paraffin Oil under the nose of viscous dissipation. Recently Mumtaz Khan *et al*. [30] explored the continuous 3D combined convective mechanism flow past a stretching perpendicular surface of uneven compactness slip effects, plunged in a permeable material congested with hybrid nanofluid (MoS_2-SiO_2/water). Afterward, Mahato *et al*. [31] studied the

effectiveness of magnetic dipole on the MHD flow of an electrically conducting hybrid nanofluid MoS_2-SiO_2/EG among two infinite perpendicular parallel plates under the nose of a rotating frame. Hussain [32] studied explorations of the flow characteristics of an ethylene-glycol-based hybrid nanofluid, including graphene-MoS_2 using numerical and statistical methods. The flows of an electro-hydrodynamic couple stress hybrid nanofluid (SWCNT-MWCNT/blood) through a stretching surface were analyzed by Anwar Saeed *et al*. [33]. In the presence of an external radial magnetic field, J Tripathi *et al*. [34] deliberated theoretical and numerical solutions of the magneto hemodynamics through a diseased artery with (Ag-Au/blood) overlapping stenosis. Hassan Waqas *et al*. [35] scrutinized the radiative flow of hybrid nanofluids containing aluminum alloys AA7072-AA7075 between two continuously rotating surfaces. A substantial influence of magnetic field on the 2D flow of couple stress hybrid nanofluid TiO_2- Ag/blood movement of combined convective mechanism across a spinning sphere in the submerging of MHD was explored by Taza Gul *et al*. [36]. H.S. Chahregh *et al*. [37] have investigated the hydrodynamic/thermal interpretation of arterial blood circulation in the appearance of titanium and silver nanoparticles. Some references are included on various topics related to MHD using nanofluid[38-53].

Inspired by the above literature, we explored the Numerical study of hybrid nanofluid (MoS_2-Fe_3O_4/Blood) flows to accomplish a stretching sheet by means of a porous medium with thermal radiation. By referring to the work of Devi and Devi. [9] a mathematical formulation of the present article flourished. The nonlinear partial differential equations of the governing flow were transformed into nonlinear ordinary differential equations, which can then be, worked out numerically employing the similarity transformation method. This study explores the effects of magnetic parameters, heat generation, radiation parameters, Eckert number, Biot number, and the effects of nanoparticle volume proportion on skin friction and the Nusselt number with temperature and velocity patterns.

2. Mathematical Analysis

Consider a steady two - dimensional flow of MoS_2-Fe_3O_4/Blood towards a porous stretching sheet under the nose of thermal radiation and magnetic field, were investigated. The system of rectilinear coordinates and the corporeal representation of the contemporary investigation are illustrated in Figure 1; the horizontal axis represents the orientation of the stretching sheet, while the vertical axis is perpendicular to the stretching sheet.

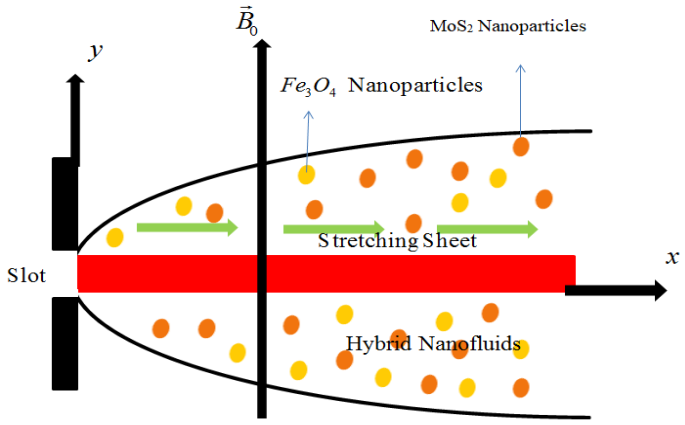

Figure 1. Physical configuration of the problem.

The stretching surface has the velocity $U_w(x) = ax$, where a denotes the constant velocity of the sheet. The wall is permeable with porous. The stretching sheet is subjected to an induced magnetic flux $\overrightarrow{B_0}$ that is orthogonal to the sheet. The sheet surface is kept at a temperature T_w that is higher than the ambient temperature T_∞.

In steady state, the presidential equations of mass, momentum, and energy, as well as the partial differential equations, can be expressed using the aforesaid considerations as the continuity equation:

$$u_x + v_y = 0 \tag{2.1}$$

$$\rho_{hnf}\left(uu_x + vu_y\right) = \mu_{hnf}u_{yy} - \sigma_{hnf}B_0{}^2u - \mu_{hnf}\frac{u}{k} \tag{2.2}$$

$$(\rho c_p)_{hnf}(uT_x + vT_y) = k_{hnf}T_{yy} - (q_r)_y + \mu_{hnf}u_y{}^2 + Q_0(T - T_\infty) \tag{2.3}$$

The boundary conditions for governing equations (2.1), (2.2), and (2.3) is:

$$u(x) = u_w(x) = ax, -k_{hnf}\frac{\partial T}{\partial y} = h_f(T_w - T),\ v(x) = 0 \text{ When } y(x) = 0 \tag{2.4}$$

$$u(x) \to 0, T \to T_\infty \text{ When } y(x) \to \infty \tag{2.5}$$

where a is a constant, the components of velocity in the x and y directions respectively, are represented by u and v, μ_{hnf} is the effective dynamic viscosity, ρ_{hnf} is the effective density, σ_{hnf} is represented by the electric conductivity, $\left(c_p\right)_{hnf}$ is the specific heat and k_{hnf} corresponds to the hybrid nanoliquid's thermal conductivity, T denote the temperature of the fluid, T_w corresponds to the wall's temperature and T_∞ denotes the ambient temperature.

Table 1. Thermo physical traits of MoS_2-Fe_3O_4/blood.

Properties	**Nanofluid**	**Hybrid Nanofluid**
Density	$\rho_{nf} = (1-\phi)\rho_f + \phi\rho_{Fe_eO_4}$	$\rho_{hnf} = (1-\phi_2)\left\{(1-\phi_1)\rho_f + \phi_1\rho_{Fe_3O_4}\right\} + \phi_2\rho_{MoS_2}$
Viscosity	$\mu_{nf} = \frac{\mu_f}{(1-\phi)^{2.5}}$	$\mu_{hnf} = \frac{\mu_f}{(1-\phi_1)^{2.5}(1-\phi_2)^{2.5}}$
Electric conductivity	$\frac{\sigma_{nf}}{\sigma_f} = \frac{\sigma_{Fe_3O_4} + 2\sigma_f - 2\phi(\sigma_f - \sigma_{Fe_3O_4})}{\sigma_{Fe_3O_4} + 2\sigma_f + \phi(\sigma_f - \sigma_{Fe_3O_4})}$	$\frac{\sigma_{hnf}}{\sigma_{bf}} = \frac{\sigma_{MoS_2} + 2\sigma_{bf} - 2\phi_2(\sigma_{bf} - \sigma_{MoS_2})}{\sigma_{MoS_2} + 2\sigma_{bf} + \phi_2(\sigma_{bf} - \sigma_{MoS_2})}$ $\frac{\sigma_{bf}}{\sigma_f} = \frac{\sigma_{Fe_3O_4} + 2\sigma_f - 2\phi_1(\sigma_f - \sigma_{Fe_3O_4})}{\sigma_{Fe_3O_4} + 2\sigma_f + \phi_1(\sigma_f - \sigma_{Fe_3O_4})}$
Heat Capacity	$(\rho c_p)_{nf} = (1-\phi)(\rho c_p)_f + \phi(\rho c_p)_{Fe_3O_4}$	$(\rho c_p)_{hnf} = (1-\phi_2)\left[(1-\phi_1)(\rho c_p)_f + \phi_1(\rho c_p)_{Fe_3O_4}\right] + \phi_2(\rho c_p)_{MoS_2}$

Properties	Nanofluid	Hybrid Nanofluid
Thermal Conductivity	$\frac{k_{nf}}{k_f}=\frac{k_{Fe_eO_4}+2k_f-2\phi(k_f-k_{Fe_eO_4})}{k_{Fe_eO_4}+2k_f+\phi(k_f-k_{Fe_eO_4})}$	$\frac{k_{hnf}}{k_{bf}}=\frac{k_{MoS_2}+2k_{bf}-2\phi_2(k_{bf}-k_{MoS_2})}{k_{MoS_2}+2k_{bf}+\phi_2(k_{bf}-k_{MoS_2})}$ $\frac{k_{bf}}{k_f}=\frac{k_{Fe_3O_4}+2k_f-2\phi_1(k_f-k_{Fe_3O_4})}{k_{Fe_3O_4}+2k_f+\phi_1(k_f-k_{Fe_3O_4})}$

Table 2. Thermophysical characteristics of MoS_2 - Fe_3O_4 /blood.

Main Features	$\rho(kg/m^3)$	$c_p(J/kgK)$	$k(W/mk)$	$\sigma(s/m)$
Blood	1060	3770	0.492	4.3×10^{-5}
Molybdenum Disulfide MoS_2	5060	397.21	904.4	2.09×10^{-4}
Ferrosoferric oxide Fe_3O_4	5200	670	6	25000

By introducing the following similarity variables:

$$u=axf'(\eta),\ v=-\left(av_f\right)^{\frac{1}{2}}f(\eta),\ \eta=\left(\frac{a}{v_f}\right)^{\frac{1}{2}}y,\ T-T_\infty=(T_w-T_\infty)\theta(\eta) \tag{2.6}$$

The emissive heat flux is expressed by means of the Rosseland approximation for radiation as:

$$q_r=-\frac{4\sigma^*}{3k^*}\frac{\partial T^4}{\partial y} \tag{2.7}$$

where the constant for Stephen-Boltzmann and the coefficient of Rosseland mean absorption are σ^* and k^*, respectively. Within the flow, temperature variations T^4 can be described as a linear function of the temperature. This is performed by expanding and eliminating the higher order terms in Taylor's series about T_∞, resulting in:

$$T^4\approx -3T_\infty^{\ 4}+4TT_\infty^{\ 3} \tag{2.8}$$

Using equations (10) and (11), Equation (3) reduces to:

$$\left(\rho c_p\right)_{hnf}\left(uT_x+vT_y\right)=k_{hnf}T_{yy}+\left(\frac{16\sigma^*T_\infty^{\ 3}}{3k^*}\right)T_{yy}+\mu_{hnf}u_y^{\ 2}+Q_0\left(T-T_\infty\right) \tag{2.9}$$

Applying the similarity variables (2.6)-(2.9) into Equations (2.1) – (2.3), the subsequent coupled ordinary differential equations are acquired, and the equation of continuity (2.1) is automatically satisfied.

$$f'''-\left(1-\phi_1\right)^{2.5}\left(1-\phi_2\right)^{2.5}\left\{\left(1-\phi_2\right)\left[\left(1-\phi_1\right)+\phi_1\left(\frac{\rho s_1}{\rho_f}\right)\right]+\phi_2\left(\frac{\rho s_2}{\rho_f}\right)\right\}\left(f'^2-ff''\right)- \\ \frac{\sigma_{hnf}}{\sigma_f}\left(1-\phi_1\right)^{2.5}\left(1-\phi_2\right)^{2.5}M^2f'-Kf'=0 \tag{2.10}$$

$$\left(\frac{k_{hnf}}{k_f}+\frac{4R}{3}\right)\theta''+\left\{(1-\phi_2)\left[(1-\phi_1)+\phi_1\left(\frac{(\rho c_p)s_1}{(\rho c_p)_f}\right)\right]+\phi_2\left(\frac{(\rho c_p)s_2}{(\rho c_p)_f}\right)\right\}\Pr f\theta'+ \quad (2.11)$$
$$(1-\phi_1)^{-2.5}(1-\phi_2)^{-2.5}P_rE_c f''^2+P_rQ\theta=0$$

Together with the dimensionless physical constraints listed below:

$$f'(0)=1,\ f(0)=0,\theta'(0)=\frac{-1}{\frac{k_{hnf}}{k_f}}B_i\left(1-\theta(0)\right),\ f'(\infty)=0,\theta(\infty)=0 \quad (2.12)$$

where the superscripts signify η-related differentiation, $M^2=\sigma_f B_0{}^2/a\rho_f$ stand for the magnetic interaction variable, $K=\nu_f/ak$, $P_r=\mu_f(c_p)_f/\kappa_f$ stand for the Prandtl number, $Q=Q_0/a(\rho c_p)_f$ represents the local heat generation, $R=4\sigma^*T_\infty{}^3/k^*k_f$ represents the radiation variable, $E_c=a^2x^2/(c_p)_f(T_w-T_\infty)$ stand for the local Eckert number and $B_i=h_f/k_f\sqrt{\frac{\nu_f}{a}}$ stand for the Boit number.

The important quantities, Skin friction coefficient, C_f , and Nusselt number, Nu_x, are given by:

$$C_f=\frac{\tau_w}{\rho_f u_w{}^2},\ Nu_x=\frac{xq_w}{k_f(T_w-T_\infty)} \quad (2.13)$$

where the heat flux, q_w and Shear stress, τ_w , distinguished as:

$$\tau_w=\mu_{hnf}\left(u_y\right)_{y=0},\ q_w=-k_{hnf}\left(T_y\right)_{y=0}+\left(q_r\right)_{y=0} \quad (2.14)$$

We get by plugging (14) into (13):

$$Cf_x\,\mathrm{Re}_x{}^{\frac{1}{2}}=\frac{f''(0)}{(1-\phi_1)^{2.5}(1-\phi_2)^{2.5}}, \quad (2.15)$$

$$Nu_x\,\mathrm{Re}_x{}^{-\frac{1}{2}}=-\left(\frac{k_{hnf}}{k_f}+\frac{4}{3}R\right)\theta'(0), \quad (2.16)$$

where Re_x, the local Reynolds number is defined as $\mathrm{Re}_x=\frac{U_w x}{\nu_f}$.

3. Results and Discussion

The numerical solution of the problem from equation (10)-(12) for MHD MoS_2-Fe_3O_4/Blood towards a porous stretching surface with effecting thermal radiation and magnetic field was performed by Matlab's integrate function referred to as bvp4c solver. The subsequent section investigates the effects of the magnetic parameter (M), porous medium (K), heat absorption (Q), Radiative parameter (R), Eckert's number (E_C), and Biot number (Bi) on velocity and temperature distribution. In this article, we discussed two types of nanoparticles, Fe_3O_4 and MoS_2, as well as blood as the base fluid (Prandtl number is Pr=21). For the allocation

of velocity and temperature, the mechanism of blood over the stretching sheet is graphically presented, along with physical parameters. The figures show that the solid line represents a hybrid nanofluid consisting of MoS_2-Fe_3O_4, while the dotted line shows Fe_3O_4. Figures 2 and 3 depict the consequences of magnetic parameter M on the velocity distribution $f'(\eta)$ and temperature distributions $\theta(\eta)$. Figure 2 depicts how velocity decreases as the magnetic parameter is increased. The transverse magnetic field generates a drag-like resistive force, which prefers to oppose fluid flow and slow down its velocity. Since the magnetic parameter enhances, the thickness of the boundary layer decreases. The velocity profile decreases as the magnetic effect rises, indicating that the magnetic field tends to slow the fluid's speed. While the fluid temperature amplifies, with an increase in magnetic values, as shown in Figure 3. Table 3 indicates that as the magnetic field rises, the skin friction coefficient declines due to the reduced velocity of the flow. Also, the magnetic field enhances the rate of heat dissipation decreases. It is pointed out that the nondimensional heat dissipation rate for MoS_2-Fe_3O_4/blood is greater than that of Fe_3O_4/blood.

Figure 4 exhibits the effect of porous media on $f'(\eta)$. The velocity of both nanofluid and hybrid nanofluid decreases as the porous media parameter is increased. Figure 5 demonstrates increasing values of the permeability coefficient as temperature rises. Figure 6 shows a temperature distribution comparison of a base fluid Blood, a nanofluid (Fe_3O_4-Blood), and a hybrid nanofluid (MoS_2-Fe_3O_4/Blood). The heat dissipation rate of MoS_2-Fe_3O_4/Blood is greater than that of Fe_3O_4/Blood and base fluid. The nanoparticles physically disperse energy as heat. The addition of more nanoparticles could increase the temperature by exerting more energy. The influence of heat absorption against dimensionless temperature is revealed in Figure 7. It is quite clear that increasing the heat absorption parameter causes an increase in temperature. These findings are qualitatively consistent with expectations, as the effect of internal heat generation is to increase the frequency of heat transport to the fluid by raising the temperature of both hybrid nanofluid and nanofluid.

The dimensionless temperature profile for the radiation parameter is plotted in Figure 8. It has been observed that the temperature profiles enhance with rising values of thermal radiation. Because the thickness of the thermal protective layer magnifies with increasing thermal radiation, the effect of thermal radiation enhances heat transfer. As a result, it is suggested that radiation be reduced in order for the cooling process to move more quickly. We also noted that the heat transfer in the case of the Fe_2O_3-Blood is comparatively less than MoS_2-Fe_3O_4/Blood. Figure 9 depicts the significance of the Eckert number. It can be seen that increasing *Ec* causes an increase in heat transfer. Figure 10 shows the effect of *Bi* on temperature profile; when viewing this figure, the temperature of MoS_2-Fe_3O_4/Blood and Fe_2O_3-Blood increases with the increasing parameter *Bi*. Table 3 shows that reduced skin friction decreases with the enlarging M, Ec, Bi, and volume fraction coefficient of Fe_3O_4. But the drag factor is indistinctly large for a hybrid Nanofluid. The proportional increases in the heat transfer rate for changes in Fe_3O_4 nanoparticles volume fraction ϕ_2 from 0.15, 0.20, 0.25, and 0.30enhance heat transfer of both nanofluid and hybrid nanofluid. This demonstrates that, compared to other traditional fluids, the hybrid nanofluid improves the heat transfer rate more efficiently.

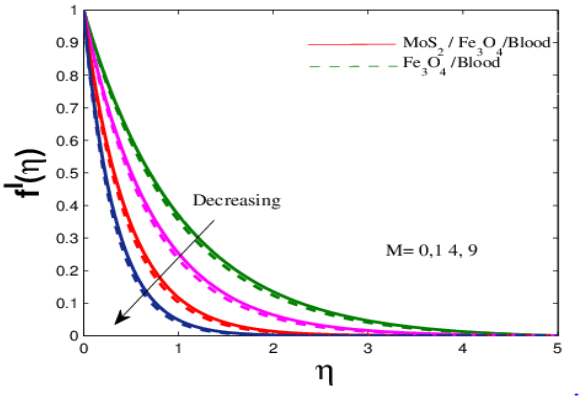

Figure 2. Effects of $f'(\eta)$ on M variations.

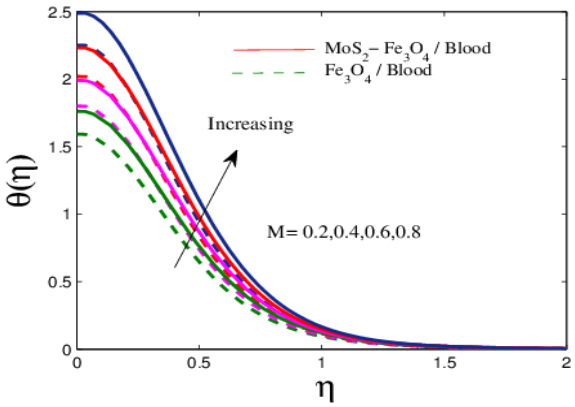

Figure 3. Effects of $\theta(\eta)$ on M adaptations.

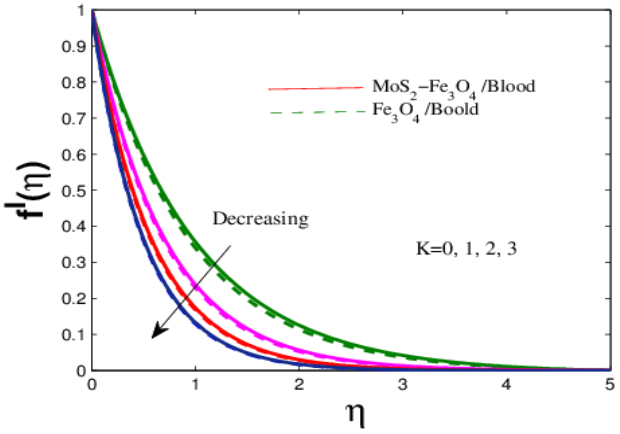

Figure 4. Effects of $f'(\eta)$ on K variations.

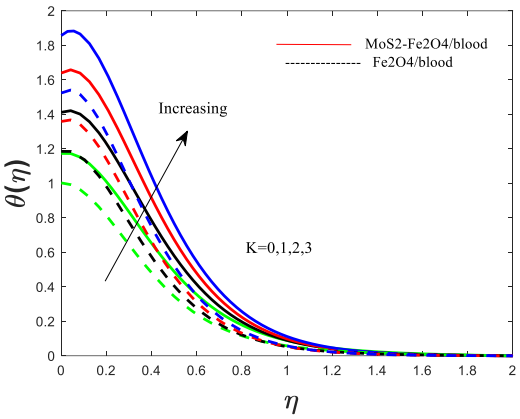

Figure 5. Effects of $\theta(\eta)$ on K variations.

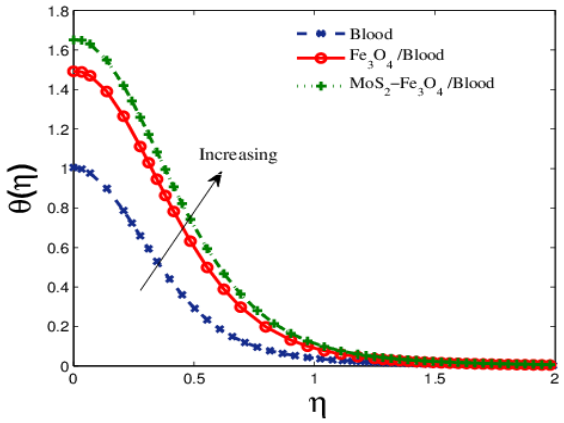

Figure 6. The effects of various Fluids.

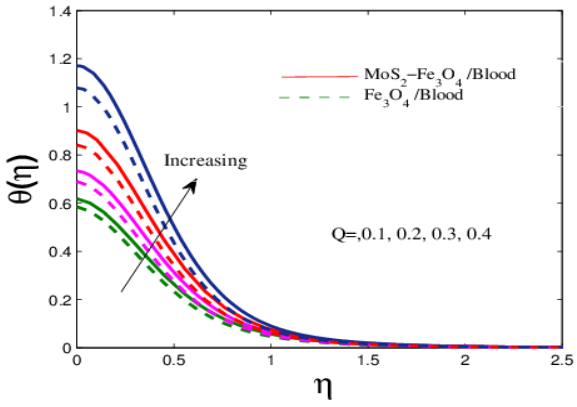

Figure 7. Impacts of Q in $\theta(\eta)$.

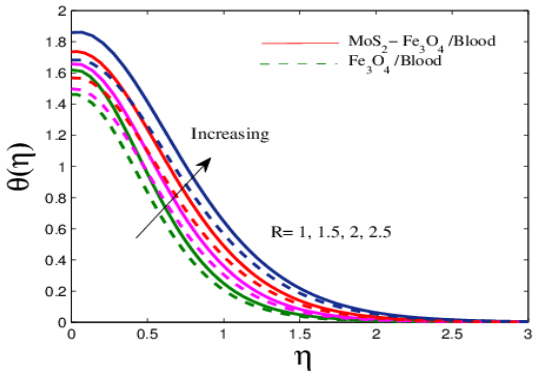

Figure 8. Consequences of R in $\theta(\eta)$.

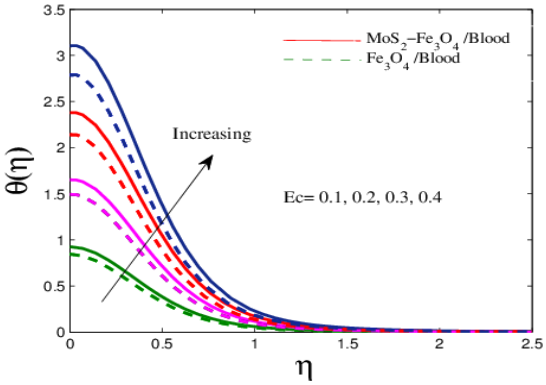

Figure 9. Consequences of Ec in $\theta(\eta)$.

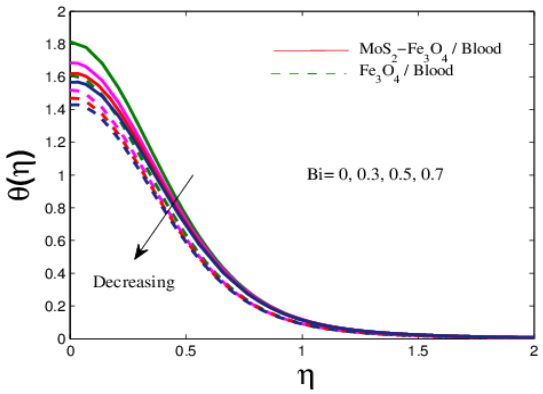

Figure 10. Consequences of Bi $\theta(\eta)$.

Table 1. $Cf_x \,\mathrm{Re}_x^{\frac{1}{2}}$ and $Nu_x \,\mathrm{Re}_x^{-\frac{1}{2}}$ for $MoS_2 - Fe_3O_4 / Blood$ and $Fe_3O_4 / Blood$.

					$Cf_x \,\mathrm{Re}_x^{\frac{1}{2}}$		$Nu_x \,\mathrm{Re}_x^{-\frac{1}{2}}$	
M	***Bi***	***R***	***Ec***	φ_2	Fe_3O_4 / *Blood*	$MoS_2 - Fe_3O_4$ / *Blood*	Fe_3O_4 / *Blood*	$MoS_2 - Fe_3O_4$ / *Blood*
1	2	0.01	0.001	0.15	-1.987448	-2.589179	1.278832	1.319292
3					-2.853769	-3.739153	1.254773	1.291414
5					-3.512798	-4.611014	1.235339	1.268787
7					-4.066390	-5.342442	1.218302	1.248877
	4				-3.799689	-4.990147	1.767688	1.838830
	6				-2.853769	-3.739153	2.149171	2.265404
0.3	8				-1.578048	-2.042269	2.477270	2.644910
		0.03			-2.853769	-3.739153	1.276455	1.309406
		0.05			-1.578048	-2.042269	1.335186	1.369804
		0.07			-1.391268	-1.791354	1.340245	1.375575
			0.002		-2.853769	-3.739153	1.260162	1.317244
			0.004		-3.512798	-4.611014	1.245637	1.262721

					$Cf_x \operatorname{Re}_x^{\frac{1}{2}}$		$Nu_x \operatorname{Re}_x^{-\frac{1}{2}}$	
M	***Bi***	***R***	***Ec***	φ_2	Fe_3O_4 / *Blood*	$MoS_2 - Fe_3O_4$ / *Blood*	Fe_3O_4 / *Blood*	$MoS_2 - Fe_3O_4$ / *Blood*
			0.006		-3.799689	-4.990147	1.209026	1.216727
				0.20	-4.310300	-5.653408	1.239496	1.269300
				0.25	-4.910118	-6.433505	1.242014	1.271446
6	2	0.02		0.30	-5.622427	-7.360897	1.244533	1.273553

4. Conclusions

In this study, a numerical investigation of MoS_2-Fe_3O_4/Blood towards a porous stretching sheet under the nose of thermal radiation and magnetic field was discovered. The impact of magnetic parameters, porous medium, heat absorption, Radiation parameter, Eckert number, Biot number, and nanoparticle volume fraction on the $Cf_x \operatorname{Re}_x^{\frac{1}{2}}$ and $Nu_x \operatorname{Re}_x^{-\frac{1}{2}}$ as well as velocity and temperature profiles has been investigated in this study. The findings are as follows: By virtue of an increase, the magnetic parameter reduces the skin friction coefficient, velocity, and Nusselt number for MoS_2-Fe_3O_4/Blood and Fe_3O_4/blood, while temperature increases; The heat transfer rate of hybrid nanofluid MoS_2-Fe_3O_4/blood is higher than those of Fe_3O_4/blood; The temperature is also increasing by increasing the heat source and radiation parameters; As the Biot number *Bi* and Eckert number *Ec* increase, so does the thermal; The skin friction values increase as the values of thermal radiation and Ec increase, whereas the frequency of occurrence of heat transfer decreases as the values of M and Ec increase.

Funding

This research received no external funding

Conflicts of Interest

The authors declare no conflict of interest

Acknowledgments

The authors would like to thank all the reviewers for their valuable comments and suggestions to improve the quality of the paper.

References

1. Choi, S. US.; Eastman, Jeffrey A. Enhancing thermal conductivity of fluids with nanoparticles. No. ANL/MSD/CP-84938; CONF-951135-29. Argonne National Lab.(ANL), Argonne, IL (United States), **1995**.
2. Sridhara, V.; Satapathy, L.N.Al2O3-based nanofluids: a review. *Nanoscale research letters* **2011,** *6*, 1-16.
3. Haile, E.; Shankar, B. A steady MHD boundary-layer flow of water-based nanofluids over a moving permeable flat plate. *Int. J. Math. Oper. Res* **2015**, *4*, 27-41, https://doi.org/10.18488/journal.24/2015.4.1/24.1.27.41.
4. Elazem, N.Y.A.; Ebaid, A.; Aly, E.H. Radiation effect of MHD on Cu water and Ag-water nanofluids flow over a stretching sheet: numerical study. *J. Appl. Computat. Math* **2015**, *4*, 1-8, https://doi.org/10.4172/2168-9679.1000235.

5. Gaikwad, S.N.; Chillal, S. Radiation effect on MHD mixed convective flow of Cu/CuO-Water nanofluids in the presence of chemical reaction. *J Nanofluids* **2018**, *7*, 509-515, https://doi.org/10.1166/jon.2018.1479.
6. Zeinali Heris, S.; Kazemi-Beydokhti, A.; Noie, S.H.; Rezvan, S. Numerical study on convective heat transfer of Al2O3/water, CuO/water and Cu/water nanofluids through square cross-section duct in laminarflow. *Eng. Appl. Comput. FluidMech* **2012**, *6*, 1-14, https://doi.org/10.1080/19942060.2012.11015398.
7. Nithyadevi, N.; Mahalakshmi, T. Numerical Study of Natural Convection Heat Transfer in a Square Enclosure with Inside Heater Utilizing Ag-Water Nanofluid. *J Nanofluids* **2017**, *6*, 1096-1110, https://doi.org/10.1166/jon.2017.1399.
8. Al-Mdallal, Q.M.; Indumathi, N.; Ganga, B.; Hakeem, A.A.. Marangoni radiative effects of hybrid-nanofluids flow past a permeable surface with inclined magnetic field. *Case Stud. Therm. Eng* **2020**, *17*, 100571, https://doi.org/10.1016/j.csite.2019.100571.
9. Devi, S.A.; Devi, S.S.U. Numerical investigation of hydromagnetic hybrid Cu–Al2O3/water nanofluid flow over a permeable stretching sheet with suction. *Int. J. Nonlinear Sci. Numer. Simul* **2016**, *17*, 249-257, https://doi.org/10.1515/ijnsns-2016-0037.
10. Rajesh, V.; Srilatha, M.; Chamkha, A.J. Hydromagnetic effects on hybrid nanofluid (Cu–Al2O3/water) flow with convective heat transfer due to a stretching sheet. *J Nanofluids* **2020**, *9*, 293-301, https://doi.org/10.1166/jon.2020.1755.
11. Waini, I.; Ishak, A.; Pop, I,. Unsteady flow and heat transfer past a stretching/shrinking sheet in a hybrid nanofluid. *Int. J. Heat Mass Transf* **2019**, *136*, 288-297, https://doi.org/10.1108/hff-05-2019-0441.
12. Alghamdi, W.; Alsubie, A.;Kumam, P.; Saeed, A.; Gul, T.. MHD hybrid nanofluid flow comprising the medication through a blood artery. *Sci. Rep* **2021**, *11*, 1-13, https://doi.org/10.1038/s41598-021-91183-6.
13. Anuar, N.S.; Bachok, N.; Pop, I.. Radiative hybrid nanofluid flow past a rotating permeable stretching/shrinking sheet. *INT J NUMER METHOD H.***2020,** https://doi.org/10.1108/hff-03-2020-0149.
14. Waini, I.; Ishak, A.; Pop, I. Hybrid nanofluid flow and heat transfer over a nonlinear permeable stretching/shrinking surface. *INT J NUMER METHOD H* **2019,** https://doi.org/10.1108/hff-01-2019-0057.
15. Wahid, N.S.; Arifin, N.M.; Khashi'ie, N.S.; Pop, I. Hybrid nanofluid slip flow over an exponentially stretching/shrinking permeable sheet with heat generation. *Mathematics* **2020**, *9*, 30, https://doi.org/10.3390/math9010030.
16. Khan, M.I.; Khan, S.A.; Hayat, T.; Waqas, M.; Alsaedi, A. Modeling and numerical simulation for flow of hybrid nanofluid (SiO2/C3H8O2) and (MoS2/C3H8O2) with entropy optimization and variable viscosity. *INT J NUMER METHOD H* **2019**,https://doi.org/10.1108/hff-10-2019-0756.
17. NurSyahirah Wahid.; NorihanMdArifin.; Najiyah Safwa Khashi'ie.; Ioan Pop. Marangoni hybrid nanofluid flow over a permeable infinite disk embedded in a porous medium.*Int. Commun. Heat Mass Transf* **2021**, *126*, 105421, https://doi.org/10.1016/j.icheatmasstransfer.2021.105421.
18. Zainal, N.A.; Nazar, R.; Naganthran, K.; Pop, I.; Unsteady EMHD stagnation point flow over a stretching/shrinking sheet in a hybrid Al2O3-Cu/H2O nanofluid. *Int. Commun. Heat Mass Transf* **2021**, *123*, 105205, https://doi.org/10.1016/j.icheatmasstransfer.2021.105205.
19. Aladdin, N.A.L.; Bachok, N.; Pop, I.. Cu-Al2O3/water hybrid nanofluid flow over a permeable moving surface in presence of hydromagnetic and suction effects. *Alex. Eng. J* **2020**, *59*, 657-666, https://doi.org/10.1016/j.aej.2020.01.028.
20. Aly, E.H.; Pop, I. Radiation and Mixed Convection Magnetohydrodynamics Boundary Layer of Hybrid Cu–Al2O3/Water Nanofluid Flow Over a Wall Jet. *J Nanofluids* **2020**, *9*, 152-160, https://doi.org/10.1166/jon.2020.1747.
21. Rajesh, V.; Chamkha, A.;Kavitha, M. Numerical investigation of Ag-CuO/water hybrid nanofluid flow past a moving oscillating cylinder with heat transfer. *Math. Methods Appl. Sci*. **2020 ,**https://doi.org/10.1002/mma.6884.
22. Babar, H.; Ali, H.M.;. Towards hybrid nanofluids: preparation, thermophysical properties, applications, and challenges. *J. Mol. Liq.***2019**, *281*, 598-633, https://doi.org/10.1016/j.molliq.2019.02.102.
23. Suresh, S.;Venkitaraj, K.P.; Selvakumar, P; Chandrasekar, M.Synthesis of Al2O3–Cu/water hybrid nanofluids using two step method and its thermo physical properties. *Colloids Surf. A Physicochem. Eng* **2011**, *388*, 41-48, https://doi.org/10.1016/j.colsurfa.2011.08.005.
24. Suresh, S.; Venkitaraj, K.P.; Selvakumar, P.; Chandrasekar, M.Effect of Al2O3–Cu/water hybrid nanofluid in heat transfer. *Experimental Thermal and Fluid Science* **2012**, *38*, 54-60, https://doi.org/10.1016/j.expthermflusci.2011.11.007.
25. Kierzenka, J.; Shampine, L.F. A BVP solver based on residual control and the Maltab PSE. *ACM TransactionsonMathematicalSoftware(TOMS)***2001**, *27*, 299-316, https://doi.org/10.1145/502800.502801.
26. Hayat, T.; Nadeem, S.; Khan, A.U. Numerical analysis of Ag–CuO/water rotating hybrid nanofluid with heat generation and absorption. *Can.J. Phy* **2019**, *97*, 644-650, https://doi.org/10.1139/cjp-2018-0011.

27. Nadeem, S.; Hayat, T.; Khan, A.U. Numerical study of 3D rotating hybrid SWCNT–MWCNT flow over a convectively heated stretching surface with heat generation/absorption. *Physica Scripta* **2019**, *94*, 075202, https://doi.org/10.1088/1402-4896/ab00b9.
28. Gu, S.H.; Nicolas, V.; Lalis, A.; Sathirapongsasuti, N.; Yanagihara, R. Complete genome sequence and molecular phylogeny of a newfound hantavirus harbored by the Doucet's musk shrew (Crocidura douceti) in Guinea. *Infection, Genetics and Evolution* **2013**, *20*, 118-123, https://doi.org/10.1016/j.molliq.2018.07.105.
29. Afridi, M.I.; Qasim, M.; Khan, N.A.; Hamdani, M. Heat transfer analysis of Cu–Al2O3–water and Cu–Al2O3–kerosene oil hybrid nanofluids in the presence of frictional heating: using 3-stage Lobatto IIIA formula. *J. Nanofluids* **2019**, *8*, 885-891, https://doi.org/10.1166/jon.2019.1626
30. Yuvaraj, T. ;Ravi, K. Multi-objective simultaneous DG and DSTATCOM allocation in radial distribution networks using cuckoo searching algorithm. *Alex. Eng. J* **2018**, *57*, 2729-2742, https://doi.org/10.1016/j.aej.2020.11.019.
31. Mahato, N.; Banerjee, S.M.; Jana, R.N.; Das, S. MoS2-SiO2/EG hybrid nanofluid transport in a rotating channel under the influence of a strong magnetic dipole (Hall effect). *Multidiscip. Model. Mater* **2020,** https://doi.org/10.1108/mmms-12-2019-0232.
32. Hussain, S.M. Dynamics of Ethylene Glycol-based Graphene and Molybdenum Disulphide Hybrid Nanofluid Over a Stretchable Surface With Velocity and Thermal Slip Conditions, **2021,** https://doi.org/10.21203/rs.3.rs-798961/v1**.**
33. Saeed, A.; Alsubie, A.; Kumam, P.; Nasir, S.; Gul, T.; Kumam, W.. Blood based hybrid nanofluid flow together with electromagnetic field and couple stresses. *Sci Rep* **2021**, *11*, 1-18, https://doi.org/10.1038/s41598-021-92186-z.
34. Tripathi, J.; Vasu, B.; Bég, O.A;. Gorla, R.S.R.. Unsteady hybrid nanoparticle-mediated magneto-hemodynamics and heat transfer through an overlapped stenotic artery: Biomedical drug delivery simulation. *Proc Inst Mech Eng H* **2021**, *235*, 1175-1196, https://doi.org/10.1177/09544119211026095.
35. Waqas, H.; Khan, S.A.; Muhammad, T. Thermal analysis of magnetized flow of AA7072-AA7075/blood-based hybrid nanofluids in a rotating channel. *Alexandria Engineering Journal* **2022**, *61*, 3059-3068, https://doi.org/10.1016/j.aej.2021.08.033.
36. Gul, T.; Ali, B.; Alghamdi, W.; Nasir, S; Saeed, A.; Kumam, P.; Mukhtar, S.; Kumam, W.; Jawad, M. Mixed convection stagnation point flow of the blood based hybrid nanofluid around a rotating sphere. *Sci Rep***2021**, *11*, 1-15, https://doi.org/10.1038/s41598-021-86868-x.
37. Chahregh, H.S.; Dinarvand, S. TiO2-Ag/blood hybrid nanofluid flow through an artery with applications of drug delivery and blood circulation in the respiratory system. *INT J NUMER METHOD H* **2020,** https://doi.org/10.1108/hff-10-2019-0732.
38. Turkyilmazoglu, M.; Pop, I.; Heat and mass transfer of unsteady natural convection flow of some nanofluids past a vertical infinite flat plate with radiation effect. *Int. J. Heat Mass Transf* **2013**, *59*, 167-171, http://dx.doi.org/10.1016/j.ijheatmasstransfer.2012.12.009.
39. Turkyilmazoglu, M.; Unsteady convection flow of some nanofluids past a moving vertical flat plate with heat transfer. *J heat transfer* **2014**, *136*, http://dx.doi.org/10.1115/1.4025730.
40. Kumar, B.R.; Kumar, T.S.; Kumar, A.G. Thermal diffusion and radiation effects on unsteady free convection flow in the presence of magnetic field fixed relative to the fluid or to the plate. *Front. Heat Mass Transf* **2015**, *6*, http://dx.doi.org/10.5098/hmt.6.12.
41. Das, S.; Jana, R.N.; Natural convective magneto-nanofluid flow and radiative heat transfer past a moving vertical plate. *Alex. Eng. J.* **2015**, *54*, 55-64, http://dx.doi.org/10.1016/j.aej.2015.01.001.
42. Mondal, P.; Mahapatra, T.R.; Parveen, R. Entropy generation in nanofluid flow due to double diffusive MHD mixed convection. *Heliyon* **2021**, *7*, e06143, https://doi.org/10.1016/j.heliyon.2021.e06143.
43. Kumar, T.P.; Uma, M.S. MHD Casson nanofluid flow over a stretching surface with melting heat transfer condition. *J Heat Transfer* **2022**, *51*, 7328-7347 https://doi.org/10.1002/htj.22646.
44. Abbas, N.; Shatanawi, W; Abodayeh, K. Computational Analysis of MHD Nonlinear Radiation Casson Hybrid Nanofluid Flow at Vertical Stretching Sheet. *Symmetry* **2022**, *14*, 1494, https://doi.org/10.3390/sym14071494.
45. Chen, J.; Chen, W.; Selim, M.M. Numerical simulation of nanofluid transportation due to MHD within a porous space. *Appl. Nanosci.* **2021**, 1-14, https://doi.org/10.1007/s13204-021-01988-0.
46. Zainal, N.A.; Nazar, R.; Naganthran, K.; Pop, I. Stability analysis of unsteady MHD rear stagnation point flow of hybrid nanofluid. *Mathematics* **2021** ,*9*, 2428, https://doi.org/10.3390/math9192428.
47. Rehman, A.; Salleh, Z. Approximate analytical analysis of unsteady MHD mixed flow of non-Newtonian hybrid nanofluid over a stretching surface. *Fluids* **2021**, *6*, 138, https://doi.org/10.3390/fluids6040138.
48. Teh, Y.Y.; Ashgar, A. Three dimensional MHD hybrid nanofluid Flow with rotating stretching/shrinking sheet and Joule heating. *CFD Lett.* **2021**, *13*, 1-19, https://doi.org/10.37934/cfdl.13.8.119.

49. Habib, D.; Salamat, N.; Abdal, S.; Siddique, I.; Salimi, M.; Ahmadian, A. On time dependent MHD nanofluid dynamics due to enlarging sheet with bioconvection and two thermal boundary conditions. *Microfluidic Nanofluidics* **2022**, *26*, 1-15, https://doi.org/10.1007/s10404-021-02514-y.
50. Gouran, S.; Mohsenian, S.; Ghasemi, S.E. Theoretical analysis on MHD nanofluid flow between two concentric cylinders using efficient computational techniques. *Alex.Eng.J.***2022,** *61*, 3237-3248, https://doi.org/10.1016/j.aej.2021.08.047.
51. Soomro, F.A.; Usman, M.; El-Sapa, S.; Hamid, M.; Haq, R.U. Numerical study of heat transfer performance of MHD Al2O3-Cu/water hybrid nanofluid flow over inclined surface. *Arch. Appl. Mech.* **2022,** 1-9, https://doi.org/10.1007/s00419-022-02214-1.
52. Ali, L.; Ali, B.; Ghori, M.B. Melting effect on Cattaneo–Christov and thermal radiation features for aligned MHD nanofluid flow comprising microorganisms to leading edge: FEM approach. *Comput. Math. with Appl.* **2022** ,*109*, 260-269, https://doi.org/10.1016/j.camwa.2022.01.009.
53. Asjad, M.I.; Sarwar, N.; Ali, B.; Hussain, S.; Sitthiwirattham, T.; Reunsumrit, J. Impact of Bioconvection and Chemical Reaction on MHD Nanofluid Flow Due to Exponential Stretching Sheet. *Symmetry* **2021**, *13*, 2334, https://doi.org/10.3390/sym13122334.